Adsorbate-substrate and adsorbate-adsorbate interactions of Na and K adlayers on Al(111)

Jörg Neugebauer and Matthias Scheffler
Fritz-Haber-Institut der Max-Planck-Gesellschaft, Faradayweg 4-6, D-1000 Berlin 33, Germany
(Received 6 April 1992)

We present total-energy, force, and electronic-structure calculations for Na and K adsorbed in various geometries on an Al(111) surface. The calculations apply density-functional theory together with the local-density approximation and the *ab initio* pseudopotential formalism. Two adsorbate meshes, namely $(\sqrt{3}\times\sqrt{3})R30°$ and (2×2), are considered and for each of them the geometry of the adlayer relative to the substrate is varied over a wide range of possibilities. By total-energy minimization we determine stable and metastable geometries. For Na we find for both adsorbate meshes that the ordering of the calculated binding energies per adatom is such that the substitutional geometry, where each Na atom replaces a surface Al atom, is most favorable and the on-top position is most unfavorable. The $(\sqrt{3}\times\sqrt{3})R30°$ structure has a lower energy than the (2×2) structure. This is shown to be a substrate effect and not an effect of the adsorbate-adsorbate interaction. In contrast to the results for Na, we find for the $(\sqrt{3}\times\sqrt{3})R30°$ K adsorption that the calculated adsorption energies for the on-top, threefold hollow, and substitutional sites are equal within the accuracy of our calculation, which is ±0.03 eV. The similarity of the energies of the on-surface adsorption sites is explained as a consequence of the bigger size of K which implies that the adatom experiences a rather small substrate electron-density corrugation. Therefore for potassium the on-top and hollow sites are close in energy already for the unrelaxed Al(111) substrate. Because the relaxation energy of the on-top site is larger than that of the threefold hollow site both sites receive practically the same adsorption energy. The unexpected possibility of surface-substitutional sites is explained as a consequence of the ionic nature of the bonding which, at higher coverages, can develop strongest when the adatom can dive into the substrate as deep as possible. The interesting result of the studied systems is that the difference in bond strengths between the "normal" and substitutional geometries is sufficiently large to kick out a surface Al atom.

I. INTRODUCTION

The adsorption of alkali-metal atoms on metal substrates has attracted significant interest in experimental as well as theoretical research for more than 150 years.[1-5] This interest is largely due to the technological importance of alkali adsorbates for efficient (i.e., low work function) electrodes and for heterogeneous catalysis (see for example Refs. 1 and 2). Furthermore, alkali metals are important candidates to study the basic mechanisms of chemisorption because they have a simple electronic structure and because it is generally assumed that alkali adsorption is not complicated by adsorbate-substrate mixing—at least for alkalis heavier than Li.

The standard way to describe alkali adsorption on metals goes back to the pioneering work of Langmuir[3] and Gurney.[4] The Langmuir-Gurney model concludes that the *isolated alkali adatom loses part of its valence electron to the metal* substrate.[4-8] With increasing coverage, however, the alkali-alkali interaction gives rise to a depolarization and reduction of the ionic nature of bonding.[9] Recently, theoretical studies[10,11] concluded that the Langmuir-Gurney model should be abandoned. It was argued that the electron transfer is small and nearly independent of coverage[10] and that the main effect is an *internal polarization* of the alkali adatom. This theoretical work[10,11] seemed to be confirmed by experimental studies.[12,13] We will not elaborate on this debate here, because it refers to the initial stage of adsorption while the present paper is concerned with higher coverages. For a more detailed discussion of these points we refer to the publications by Scheffler *et al.*[8] and King and Benesh.[14] What is interesting at this point is that the existence of such debate demonstrates that the understanding of chemisorption processes is still at its infancy.

With respect to the other, generally applied assumption, namely that intermixing with the substrate will not occur and that alkalis like Na or K adsorbed on a close-packed metal surface will occupy a high-coordination site on the practically unperturbed surface, we recently learned from our total-energy calculations[15] that this is not correct. Experimental studies using surface-extended x-ray-absorption fine structure (SEXAFS)[15] and core-level spectroscopy[16] confirmed this finding. In the present paper we give a more detailed description of our earlier theoretical work on Na $(\sqrt{3}\times\sqrt{3})R30°$ on Al(111) and we extend our study to the low-coverage (2×2) structure and to potassium adlayers.

The outline of the present paper is as follows. In Sec. II we summarize some details of our theoretical approach. After defining the basis set and the *ab initio* pseudopotentials in Sec. II A, we describe in Sec. II B a method which enables us to treat external electrostatic fields within the supercell formalism. This method helps to improve the efficiency of the calculations, and in particular it can be used to treat general external electrostatic fields and their effects on surfaces, which is relevant for example in field-ion microscopy. The merits of the

method and how it can be used for adsorbate calculations are discussed in Sec. II C. Sections III and IV then describe the results for the chemisorption of Na and K. We start with some definitions (Sec. III A), and in Sec. III B we discuss the binding energies and geometries for $(\sqrt{3}\times\sqrt{3})R30°$ Na on Al(111). In Sec. III C we compare these results with those of a $\Theta=\frac{1}{4}$ (2×2) structure, and in Sec. III D a simple physical model is proposed which explains the different nature of the "normal" and the new, substitutional adsorption of alkalis. To learn more about chemical trends we compare in Sec. IV the differences in the adsorption of Na with that of K using the same overlayer meshes. In Sec. V we summarize our results. All equations in this paper are given in atomic units, i.e., energies are in hartrees and lengths are in bohrs.

II. THEORETICAL METHOD

A. Pseudopotentials and basis set

The calculations described below are based on the density-functional theory (DFT) using the local-density approximation (LDA) for the exchange-correlation functional.[17,18] The wave functions are expanded in a plane-wave basis set and the electron-ion interaction is described by *ab initio* ionic pseudopotentials.[19] The clean and adsorbate covered Al(111) surfaces are modeled by supercells taking a slab with up to ten aluminum layers. Because of our new approach, which is described in Sec. II B, such a ten-layer substrate gives practically the same results as a four-layer substrate. Therefore most calculations are done with the thinner slab. The thickness of the vacuum region is taken equivalent to a thickness of seven Al layers.

The ionic pseudopotentials are represented by fully separable, norm-conserving *ab initio* pseudopotentials[20] as given by Gonze, Stumpf, and Scheffler.[19] These pseudopotentials are written in terms of s and p projection operators plus a local component,

$$V^{\text{pseudo}}(r,r')=V^{\text{local}}(r)\delta(r-r')+\sum_{l=0}^{1}V_l(r)V_l(r')\hat{P}_l \ . \quad (1)$$

Here $\delta(r-r')$ is the Dirac δ function. The pseudopotential of Eq. (1) is correct for the s, p, and d components (for details see Ref. 19). For $l\geq3$ the correct potential is replaced by the d potential. With this pseudopotential we get a basis-set-converged calculation for bulk aluminum with an energy cutoff of the plane-wave basis set of $E^{\text{cut}}=20$ Ry. Using a single-atom bulk unit cell and 182 Monkhorst-Pack special $\mathbf{k}$ points[21] in the irreducible part of the Brillouin zone we obtain the lattice constant $a_0=3.95$ Å, the bulk modulus $B_0(a_0)=0.78$ Mbar and the cohesive energy $E_{\text{coh}}=4.14$ eV. In these results the zero-point vibrations are taken into account.[22] They increase the *directly* calculated lattice constant by 0.4%. Neglecting zero-point vibrations we would get $\bar{a}_0=3.94$ Å and $B_0(\bar{a}_0)=0.79$ Mbar. For the cohesive energy the free atom is treated by a big cubic supercell ($a=9.0$ Å) using the LDA and adding the spin-polarization energy $E^{\text{LSDA}}-E^{\text{LDA}}=-0.15$ eV.

The theoretical results are in good agreement with the experimental values of bulk aluminum. These are $a_0^{\text{exp}}=4.02$ Å, $B_0^{\text{exp}}(a_0^{\text{exp}})=0.76$ Mbar, and $E_{\text{coh}}^{\text{exp}}=3.40$ eV.[23] It is interesting to note that even for the nearly free electron metal aluminum, d orbitals play some role for the chemical bonding. This can be seen in the influence of the d component of the aluminum pseudopotential. If we replace the potential given in Eq. (1) by one which is only correct for the s and p components, the calculated lattice constant becomes too large: $\bar{a}_0=4.13$ Å.

For the surface calculations the just-described extreme cases for E^{cut} and $\mathbf{k}$-point sampling are not feasible. We therefore used $E^{\text{cut}}=8$ Ry and a $\mathbf{k}$ sampling which takes six special $\mathbf{k}$ points[24] in the irreducible part of the two-dimensional Brillouin zones of Al(111) $(\sqrt{3}\times\sqrt{3})R30°$ and the (2×2) surface into account (see Fig. 1). In the [111] direction the Brillouin zone of the slab is very flat. Therefore the $\mathbf{k}$ integration in this direction is performed using the midpoint formula. The lattice constant, bulk modulus, and cohesive energy of this calculation are 1.0%, 4.4%, and 0.6% bigger than those of the fully basis-set- and $\mathbf{k}$-sampling-converged calculations. We therefore conclude that our choices of E^{cut} and $\mathbf{k}$ sampling give a reliable description of the structural and elastic properties.

In the following we use these choices of E^{cut} and $\mathbf{k}$ sampling and we neglect zero-point vibrations. The corresponding lattice constant of aluminum then is $\bar{a}_0=3.98$ Å. For our adsorption calculations we take this value for the substrate in order to avoid artificial stress in the slab.

For the alkali adsorbate a proper treatment of the core-valence exchange-correlation functional is known to be important.[25–27] We use the same treatment as described in Ref. 27. In order to stabilize the convergence, the electronic states were occupied according to a Fermi distribution $f(\epsilon,T^{\text{el}})$ with a half-width $k_BT^{\text{el}}=0.1$ eV. Therefore the functional which is minimized with respect to $n(\mathbf{r})$ is not the total energy $E[n(\mathbf{r})]$ but the free energy

$$F[n]=E[n]-T^{\text{el}}S^{\text{el}} \ , \quad (2)$$

with the entropy[28]

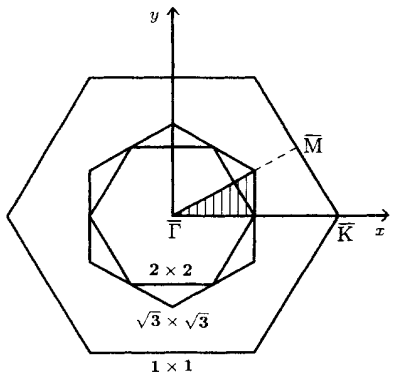

FIG. 1. Surface Brillouin zone (BZ) for the (1×1), $(\sqrt{3}\times\sqrt{3})R30°$ and (2×2) surface structures of fcc(111). The irreducible part of the BZ $(\sqrt{3}\times\sqrt{3})R30°$ for adsorption sites having C_{3v} symmetry is hatched.

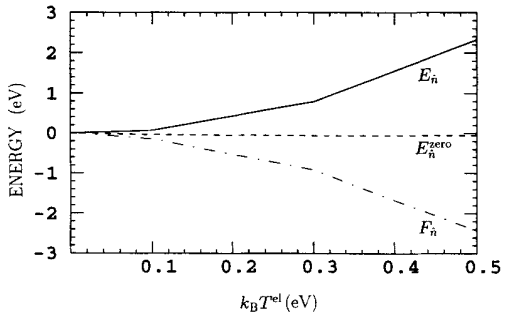

FIG. 2. Total energy $E_{\hat{n}}$, zero energy $E^{\text{zero}}_{\hat{n}}$, and free energy $F_{\hat{n}}$ vs $k_B T^{\text{el}}$ for the substitutional adsorption of $(\sqrt{3}\times\sqrt{3})R30°$ Na on Al(111).

$$S^{\text{el}} = -2k_B \sum_i [f_i \ln f_i + (1-f_i)\ln(1-f_i)] - S_0 \ , \qquad (3)$$

where k_B is the Boltzmann constant and $f_i = f(\epsilon_i, T^{\text{el}})$ is the occupation number of the ith state. S_0 is chosen such that the entropy S^{el} vanishes for $T^{\text{el}}=0$ K. We denote the density at the minimum of $F[n]$ as $\hat{n}(\mathbf{r})$. In order to find the equilibrium position we minimize the function $F_{\hat{n}}(\{\mathbf{R}_I\})$. A better treatment would be to minimize the function $E^{\text{zero}}_{\hat{n}}(\{\mathbf{R}_I\}) = E_{\hat{n}}(\{\mathbf{R}_I\}) - T^{\text{el}}S^{\text{el}}/2$, which equals the total energy at zero temperature with an error of the order of $O[(T^{\text{el}})^3]$.[29] Figure 2 gives a numerical proof of this relation and it shows that $O[(T^{\text{el}})^3]$ is indeed a small quantity for the interesting value $k_B T^{\text{el}} \approx 0.1$ eV. For the small values of $k_B T^{\text{el}}$ used in our calculations both functions $F_{\hat{n}}(\{\mathbf{R}_I\})$ and $E^{\text{zero}}_{\hat{n}}(\{\mathbf{R}_I\})$ give practically the same geometry. For calculated binding energies, however, we give below the results of $E^{\text{zero}}_{\hat{n}}$.

The free-energy function $F[n]$ is minimized by applying a Car-Parrinello-like molecular-dynamics technique on the single-particle wave functions.[30] Simultaneously, the adsorbate and the atoms of the two top substrate layers are relaxed according to an "optimized steepest descent approach":[31] At each step of the iteration this approach takes the forces on the atoms into account together with their damped velocity, which is obtained from the previous iteration.

B. Treatment of an external electrostatic field

In order to improve the numerical efficiency of supercell calculations it is desirable to reduce the number of atoms per cell without losing the required accuracy of the calculations. For surface calculations which are modeled by a slab it would be advantageous to reduce the slab thickness. For structural and elastic properties of clean, unreconstructed fcc(111) surfaces it is usually sufficient to use four-layer-thick slabs (see Sec. II C). For adsorbate systems the adsorbate-induced surface-dipole and work-function changes usually make it necessary to adsorb on both sides of the slab. Unfortunately, this often requires using thicker slabs in order to reduce the though-slab adsorbate-adsorbate interaction. Typical slab thicknesses are then between eight and twelve substrate layers.

In Fig. 3 we show the electrostatic (dashed curve) and

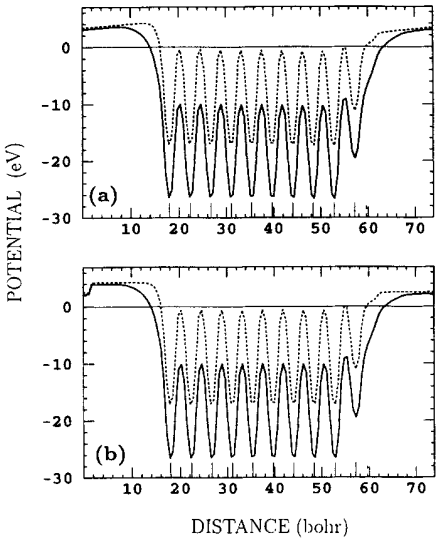

FIG. 3. (a) xy-averaged (parallel to the surface) electrostatic potential (dashed line) and effective potential (solid line) for a ten-layer Al slab with Na adsorbed at the surface-substitutional site ($\Theta=\frac{1}{3}$). The solid vertical lines mark the positions of the Al layers in the slab, the vertical dashed line marks the position of the Na overlayer. Note that a strong electrostatic field is induced in the whole vacuum region. (b) The same as in (a), but with dipole correction visible as a potential jump which separates the work functions of the clean and adsorbate-covered surfaces.

the effective potential (full curve) of a slab calculation with an adsorbate layer on the right side only. Figure 3(a) shows the results of a supercell calculation where no precaution is taken to avoid the artificial macroscopic electrostatic field which arises due to the periodic boundary conditions. In order to avoid this artificial field we introduce a planar dipole layer in the middle of the vacuum region. Its dipole strength is calculated self-consistently such that the adsorbate-induced dipole is compensated for. The resulting electrostatic and effective potentials of the slab are shown in Fig. 3(b), where the added dipole layer can be seen on the left side of the figure. With this treatment the artificial electrostatic interaction between the surfaces through the vacuum region is canceled. As a consequence the slab thickness can be reduced, which improves the efficiency and accuracy of the calculations (see Sec. II C). Note that the computer time scales as M^{ξ} where M is the number of atoms per super cell and ξ is between 2 and 3. Thus, for a $\frac{1}{3}$ coverage adlayer it is a significant gain if one can replace a ten-layer slab (which has $M=30$ atoms/cell) by a four-layer slab (which has $M=12$ atoms/cell).

We like to mention that the same method can be used to treat the interaction of a true external electrostatic field with a surface which, for example, is relevant in field-ion microscopy. The following description is therefore kept general, i.e., we will not specify if the external field is introduced in order to compensate for an artificial supercell-induced field or if it is due to an external physical electrode. In a first step we investigate the modifications of the total energy and forces due to the in-

troduction of an external electrostatic field

$$\mathcal{E}(\mathbf{r}) = -\nabla\phi^{\text{ext}}(\mathbf{r}) , \tag{4}$$

with $\phi^{\text{ext}}(\mathbf{r})$ the external electrostatic potential. We define the change of the Kohn-Sham Hamiltonian as

$$\Delta h = \phi^{\text{ext}}(\mathbf{r}) - \phi_0 , \tag{5}$$

where the constant ϕ_0 describes the interaction of the potential $\phi^{\text{ext}}(\mathbf{r})$ with the ionic pseudopotentials:

$$\phi_0 = \frac{\sum_I Z_I \phi^{\text{ext}}(\mathbf{R}_I)}{\sum_I Z_I} . \tag{6}$$

Z_I is the valency of the Ith pseudopotential and ϕ^{ext} is due to an external electrostatic field which originates outside the atomic slab. It is therefore constant over the range of an atomic core radius.

It is convenient to include the field-ion interaction in the Kohn-Sham Hamiltonian and not to modify $E^{\text{ion-ion}}$. But this could also be formulated differently. The additional part in the Hamiltonian changes the free-energy functional

$$F[n(\mathbf{r})] = T[n] + E^{e\text{-}e}[n] + \int V^{\text{ion}}(\mathbf{r}) n(\mathbf{r}) d\mathbf{r} + E^{\text{ion-ion}} - T^{\text{el}} S^{\text{el}} \tag{7}$$

to

$$\tilde{F}[n(\mathbf{r})] = F[n(\mathbf{r})] + \Delta E[n(\mathbf{r})] . \tag{8}$$

Here $T[n], E^{e\text{-}e}, E^{\text{ion-ion}}$ are the kinetic, electron-electron, and ion-ion interaction energy. $V^{\text{ion}}(\mathbf{r})$ is the ionic pseudopotential and $\Delta E[n]$ is

$$\Delta E[n(\mathbf{r})] = \int \Delta h(\mathbf{r}) n(\mathbf{r}) d\mathbf{r} = \int \phi^{\text{ext}}(\mathbf{r}) n(\mathbf{r}) d\mathbf{r} - \sum_J Z_J \phi^{\text{ext}}(\mathbf{R}_J) . \tag{9}$$

The force acting on the Ith nucleus is then

$$\mathbf{F}_I[n] = -\frac{\partial \tilde{F}}{\partial \mathbf{R}_I} = -\int \frac{\delta \tilde{F}}{\delta n} \frac{\partial n}{\partial \mathbf{R}_I} d\mathbf{r} - \int \frac{\partial V^{\text{ion}}}{\partial \mathbf{R}_I} n(\mathbf{r}) d\mathbf{r} - \frac{\partial E^{\text{ion-ion}}}{\partial \mathbf{R}_I} + \Delta F_I , \tag{10}$$

with

$$\Delta \mathbf{F}_I[n] = -\frac{\partial \Delta E}{\partial \mathbf{R}_I} = -\sum_J Z_J \frac{\partial \phi^{\text{ext}}(\mathbf{R}_J)}{\partial \mathbf{R}_I} = -Z_I \mathcal{E}(\mathbf{R}_I) , \tag{11}$$

which is simply the force acting on a charge Z_I due to the field $\mathcal{E}$. The first part of $\mathbf{F}_I[n]$ in Eq. (10) vanishes for the self-consistent charge density $\hat{n}$, since $\tilde{F}[\hat{n}]$ then is the minimum.

By this method we can handle the above-mentioned problem of adsorbate-induced dipoles as well as the influence of external electric fields which are relevant, for example, in field-ion or scanning-tunneling microscopy. This is illustrated in Fig. 4, where the effective potential and the charge-density change induced by the applied constant electric field $\mathcal{E} = 10^{10}$ V/m are shown. This is a typical field used for the field desorption of alkali atoms adsorbed on metal surfaces.[32] As expected, the field is rapidly screened inside the metallic slab [Fig. 4(b)]. Figures 4(c) and 5 show the screening electron density of the adsorbate covered surface for the on-surface adsorption (xy averaged) and for the substitutional adsorption (a cut perpendicular to the surface). In both cases we find a decrease of the surface electron density on the vacuum side of the adlayer and that the interface region between Na and Al is changed little.

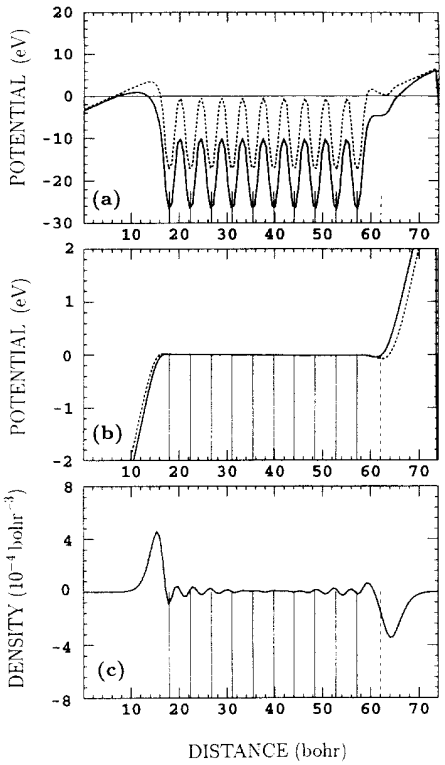

FIG. 4. (a) xy-averaged (parallel to the surface) electrostatic potential (dashed line) and effective potential (solid line) for a ten-layer Al slab covered on one side with a $\Theta = \frac{1}{3}$ Na monolayer at the fcc site within a strong electrostatic field of $\mathcal{E} = 10^{10}$ V/m perpendicular to the surface. The solid vertical lines mark the positions of the Al layers in the slab, the vertical dashed line marks the position of the Na overlayer. (b) Changes in the electrostatic (dashed) and effective (solid line) potential due to the applied electrostatic field. (c) Electron-density change $\Delta\hat{n}(z)$ induced by the electrostatic field. The main changes occur at the slab surfaces. Inside the slab Friedel-like oscillations can be seen.

It may be interesting to compare our method to that of Inglesfield.[33] The main difference is that his approach considers a semi-infinite substrate with two-dimensional translational symmetry whereas we take a slab system with a finite number of layers. This means that in our case the number of electrons is fixed, so that the system is always neutral, while in Inglesfield's method the bulk Fermi level is kept constant so that the number of electrons is changed. Thus the charge depletion and accumu-

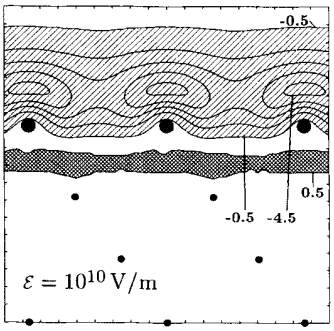

FIG. 5. Electron-density change $\Delta\hat{n}(z)$ induced by an electrostatic field $\mathcal{E}=10^{10}$ V/m for $(\sqrt{3}\times\sqrt{3})R30°$ Na on Al(111) (substitutional site). The figure shows contours in the plane lying normal to the surface and parallel to the $[1\bar{2}1]$ axis (see also Fig. 7). Contours are separated by 0.5×10^{-4} bohr^{-3}. The substrate Al atoms are indicated by small dots, the Na adsorbate by large dots. The contour units are 10^{-4} bohr^{-3}.

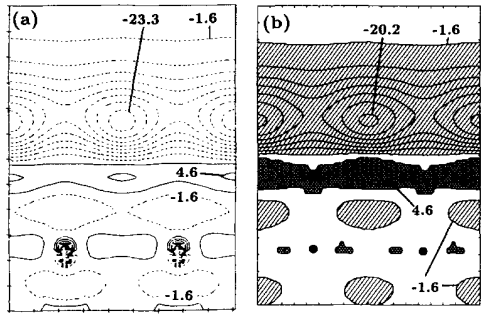

FIG. 6. Comparison of the screening charge densities calculated by (a) Inglesfield (Ref. 33) and (b) by us for the Al(100) surface. The external electric field is $\mathcal{E}=5.14\times10^{9}$ V/m. The figure shows contours in the plane lying normal to the surface which intersects the atoms in the second surface layer. The first contours are $\pm1.6\times10^{-5}$ bohr^{-3}. Contours are separated by 3.1×10^{-5} bohr^{-3}. In (a) dashed contours indicate negative electron density and the solid contours positive density. For our calculation we used a ten-layer Al substrate. The atomic positions are marked by dots.

lation due to the electric field is realized in our system by a charge transfer from one surface to the other. This can be seen in Fig. 4(c), which also shows that the charge-density change occurs only in a small region at the two surfaces and that the field is efficiently screened inside the slab, as one would expect for a metal. As a consequence there is no change of the charge density inside the slab, with the exception of small-amplitude Friedel oscillations. A further difference to Inglesfield's scheme occurs because we calculate the response of the electronic system on an external potential $\phi^{\text{ext}}(\mathbf{r})$ defined in the whole supercell whereas Inglesfield considers only a smaller (e.g., two-layers thick) surface region and applies boundary conditions. Nevertheless the physics described by both methods should be the same. Figure 6 shows that both methods give nearly the same results for the field-induced electron-density change. The technical differences are related only to a more or less efficient energy minimization. We believe that for many systems our method is more efficient and possibly also more accurate. Exceptions are systems which contain first row elements (e.g., oxygen) or $3d$ transition metals. For these systems Inglesfield's approach should be clearly more efficient.

Let us now apply our method to the dipole correction of an adsorbate covered surface. We consider a supercell given by the three lattice vectors $\mathbf{a}_1$, $\mathbf{a}_2$, and $\mathbf{a}_3$, where $\mathbf{a}_3$ is perpendicular on the surface (parallel to the z axis) and $\mathbf{a}_1$ and $\mathbf{a}_2$ are parallel to the surface. The area of the two-dimensional surface unit cell is $A=|\mathbf{a}_1\times\mathbf{a}_2|$ and the unit-cell volume is $\Omega=\mathbf{a}_1(\mathbf{a}_2\times\mathbf{a}_3)$, with the laterally averaged charge density

$$n(z)=\frac{1}{A}\int_A n(x,y,z)\,dx\,dy\ , \tag{12}$$

and the z value where the averaged charge density is minimal in the supercell is called z_0 (z_0 is in the vacuum region). The dipole moment μ per area A of the slab is then given by

$$\mu=\int_{z_0}^{a_3+z_0} n(z)z\,dz-\sum_I Z_I z_I\ . \tag{13}$$

z_I is the z component of $\mathbf{R}_I$ on the z axis. This dipole moment is compensated by a dipole layer placed at z_0 parallel to the surface, which gives rise to an electrostatic potential

$$\phi^{\text{ext}}(\mathbf{r})=-\frac{4\pi\mu}{\Omega}[z-a_3\Theta(z_0-z)],\quad 0\le z<a_3\ . \tag{14}$$

The potential ϕ^{ext} corresponds to a homogeneous electric field $\mathcal{E}=\mu/4\pi\Omega$ parallel to the z-axis. The change in total energy according to Eq. (9) is

$$\Delta E=-\mu\mathcal{E}\ , \tag{15}$$

which is the interaction energy of a dipole μ with an electrostatic field $\mathcal{E}$. In order to check the consequences of the dipole correction we compared total energy, charge density, and effective potential with and without this correction for a ten-layer Al slab covered on one side with a $\Theta=\frac{1}{3}$ monolayer Na at the substitutional site. The vacuum potentials of the adsorbed and clean surface are now separated by the dipole layer [Fig. 3(b)], i.e., the potential jump is just the change in work function due to the adsorbate-induced surface dipole. As expected, the total energy for the system with the dipole correction is lower, but the energy difference is small (14 meV) and stems partly (5 meV) from the interaction energy of a dipole in an electrostatic field according to Eq. (15) and partly (9 meV) from the redistribution of the electrons. The small size of the total-energy change can be understood because the charge transfer is very small. It is interesting to note that the field-induced electron-density changes (polarization) are much smaller than those induced by an adsorbatelike Na [compare Fig. 4(c) and Fig. 12].

Generally one can say that neglecting the dipole correction even for systems with a large surface dipole such as Na on Al results in a small change of the binding energy of some tens of meV. However, a correct treat-

TABLE I. Formation energy of the $(\sqrt{3}\times\sqrt{3})R30°$ surface-vacancy and adsorption energy of Na on Al(111). We consider different layer thicknesses and the situations where both surfaces [marked by (2)] and only one surface [marked by (1)] are perturbed. For the adsorbate the fcc, on-top, and substitutional sites are considered. The Na position is relaxed but the aluminum atoms are kept frozen at the perfect-lattice geometry. The energies are given in eV.

layers	vac(2)	vac(1)	fcc(1)	top(2)	top(1)	sub(2)	sub(1)
4	0.288	0.407	−1.406	−1.285	−1.280	−1.605	−1.567
7	0.494	0.568	−1.403	−1.297	−1.281	−1.526	−1.428
10	0.389	0.389	−1.386	−1.290	−1.274	−1.578	−1.568

ment is not very difficult and for the calculated work function it is in fact of high importance.

C. Calculations to determine the required slab thickness and other tests

In this section we show how the above-described method can be used to improve the efficiency of surface calculations. Thus, the external field will be the field introduced in order to cancel the long-range dipole field due to an asymmetric slab.

Since a surface vacancy as well as a substitutional adsorbate represents a relatively strong perturbation, the question arises how many atomic layers are necessary for the slab in order to properly model a realistic surface. In this respect it is important to study the differences for the adsorption on one and two sides of the slab. We therefore calculated the binding energies for the top, fcc, and substitutional sites, and additionally for the surface vacancy, putting the sodium (or vacancy) on one and on both sides of the slab. We consider a $(\sqrt{3}\times\sqrt{3})R30°$ adsorbate (or vacancy) structure and in order to take advantage of C_{3v} symmetry we choose four-, seven-, and ten-layer aluminum slabs. For the fcc site the C_{3v} symmetry is then only retained if we adsorb on one side. As these calculations are aimed to test the effects of slab thickness we optimized the height of the adatom only and kept the aluminum atoms frozen at their perfect lattice positions. The resulting total energies are listed in Table I. For small slabs the greatest vacancy formation energy differences occur between the two situations [denoted by vac(1) and vac(2)] in which the vacancy is created on one or on both sides: the difference is 0.12 eV for the four-layer slab. For a ten-layer slab both energies are identical. With respect to total energies for "normal" adsorption sites, i.e., for the fcc and on-top positions, the comparable difference (0.05 eV) for a four-layer slab indicates that such a slab is thick enough regardless of adsorbing on one or two sides. We emphasize, however, that this conclusion holds for a fcc(111) metal surface, for which no strong surface relaxation or reconstruction occurs. For the substitutional site and the surface vacancy a four-layer slab yields correct binding energies within 20 meV only if one adsorbs on one side. The differences in binding energy for the adsorption on one and two sides of a ten-layer slab which are about 10 meV are due to numerical inaccuracies.

TABLE II. Change of the bandwidth of occupied states in eV for the uncovered (clean) slab and of $(\sqrt{3}\times\sqrt{3})R30°$ Na at fcc, on-top, and substitutional sites adsorbed on one (1) and on two (2) sides of slabs consisting of 4, 7, and 10 layers of Al(111). As a reference energy we use the result for the clean ten-layer Al(111) slab. The Na position is relaxed but the aluminum atoms are kept frozen at the perfect-lattice geometry. All energies are in eV.

layers	clean	fcc(1)	top(2)	top(1)	sub(2)	sub(1)
4	−0.321	−0.324	−0.348	−0.305	−0.573	−0.443
7	−0.127	−0.124	−0.109	−0.108	−0.153	−0.141
10	=0	−0.001	−0.126	−0.038	−0.007	−0.011

TABLE III. Convergence tests for adsorption energies (in eV) per adatom with respect to basis set (plane-wave energy cutoff, $E^{\rm cut}$), **k**-point sampling, width of the vacuum region, and Fermi-distribution width ($k_BT^{\rm el}$). The substrate consists of a four-layer Al(111) slab. The Na position is relaxed but the aluminum atoms are kept frozen at the perfect-lattice geometry.

$E^{\rm cut}$ (Ry)	**k** points	vacuum (Å)	$k_BT^{\rm el}$ (eV)	fcc(1) (eV)	top(1) (eV)	sub(1) (eV)
8	6	16.1	0.1	−1.406	−1.280	−1.567
8	6	16.1	0.3	−1.405	−1.281	−1.549
12	6	16.1	0.3	−1.405	−1.284	−1.577
8	42	16.1	0.3	−1.404	−1.289	−1.622
8	6	23.0	0.3	−1.407	−1.290	−1.547

We also investigated how atomic forces and the bandwidth of the occupied states depend on the slab thickness and on the adsorption. The forces on the aluminum atoms differ between the one-side and two-side perturbations for all slabs by less than 10^{-3} hartree/bohr. The changes of the bandwidth are listed in Table II. It can be seen that with increasing slab thickness the bandwidth increases. In other words, the bottom of the band shifts to lower energies when referred to the Fermi level. This effect is understood as a quantum-size effect: The wave function of the lowest level is a bonding state which spreads over the whole slab. Obviously it gets more extended when the slab gets thicker and as a consequence its kinetic energy is lowered.

Finally we mention some tests which concern the basis-set convergence, **k** sampling, Fermi-function width, and the thickness of the vacuum region. We increased the plane-wave basis set up to an energy cut off of 12 Ry, the number of special **k** points to 42, the Fermi width to $k_BT^{\rm el}=0.3$ eV, and the vacuum region to a width equivalent to that of nine Al layers. The aluminum slab had four fcc(111) layers and the adsorbate was put only on one side. The differences in binding energies for the different calculations were always smaller than 50 meV (see Table III).

III. Na ADSORPTION

A. Introduction

So far it has been usually assumed that an alkali adatom on close-packed metal surfaces will occupy the high

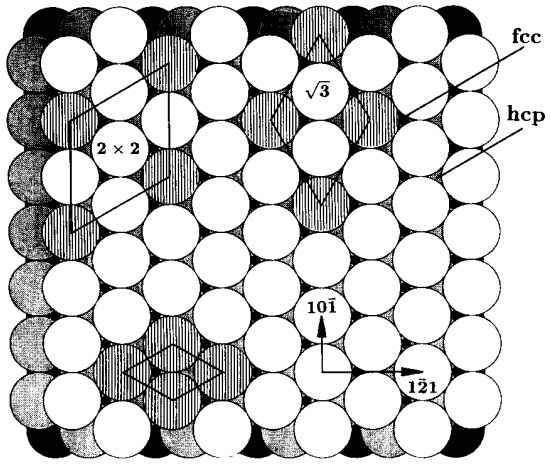

FIG. 7. The (1×1), $(\sqrt{3}\times\sqrt{3})R30°$, and (2×2) surface unit cells of Al(111). White, grey, and black circles show the top, second, and third layer of Al. Edge atoms of the three unit cells are hatched. Furthermore, the fcc and hcp on-surface adsorption sites are indicated.

coordination site on the practically undistorted substrate. For a fcc(111) substrate this would be the threefold-coordinated fcc hollow or hcp hollow site (see Fig. 7). In the following we will discuss these sites but we will also discuss the on-top and substitutional positions. Because the surface-substitutional site has been completely disregarded, we call the other adsorption sites "normal" or "on-surface" sites to distinguish them from the new situation, which also may be called a "surface alloy." Note that for aluminum no bulk alloys exist with Na or K. This is in fact plausible because the atomic radii are quite different: For Al we have $r^{\mathrm{Al}}=1.42$ Å, and for Na and K we have $r^{\mathrm{Na}}=1.83$ Å and $r^{\mathrm{K}}=2.26$ Å, respectively.[34] At the surface the size constraint is relaxed and therefore a "surface alloy" could become possible. Thus, the alkali may replace a surface aluminum atom by displacing the atom to a new position on top of the adlayer, or by causing it to diffuse away to a step position. Figure 7 shows the top view at the surface with three different surface unit cells.

In order to compare the energetics of the surface-substitutional adsorption with that of the "normal" adsorption it is necessary to define what we will call the *adsorption energy per adatom*. For the on-surface adsorption this is defined as

$$E_{\mathrm{ad}}^{\mathrm{Na/Al(111)}}=E^{\mathrm{Na/Al(111)}}-(E^{\mathrm{Al(111)}}+E^{\mathrm{Na\text{-}atom}}) , \tag{16}$$

where $E^{\mathrm{Na/Al(111)}}$ is the total energy per adatom, $E^{\mathrm{Al(111)}}$ is the corresponding energy of the clean Al(111) slab, and $E^{\mathrm{Na\text{-}atom}}$ is the total energy of a free Na atom.

For the surface-substitutional site the definition of the adsorption energy is slightly more complicated. We will consider the chemical reaction where the replaced Al atom has moved to a step. Because a chemical-reaction energy is independent of the reaction path we can separate the substitutional adsorption into two hypothetically independent processes. The first one is the creation of a $(\sqrt{3}\times\sqrt{3})R30°$ surface-vacancy structure, and the second process is the chemisorption of the alkali adlayer on this vacancy-rich surface.

The formation energy of a vacancy is the lowest energy to remove an atom from the surface, and usually the atom is brought to a *reservoir* which determines the atomic chemical potential. For crystals built from only a single species the chemical potential is the cohesive energy. The physics behind this is that the removed atom is brought to a step or kink site at the surface. By this process the surface is essentially reproduced, i.e., the macroscopic number of step and kink sites is not changed. In other words, adsorbing an Al atom at a kink site of a realistic Al surface releases an energy equal to the bulk cohesive energy. The formation energy of the surface-vacancy structure then is

$$E_f^{\mathrm{vac}}=E^{\mathrm{vac}}+(E^{\mathrm{Al\text{-}atom}}-E_{\mathrm{coh}})-E^{\mathrm{Al(111)}} . \tag{17}$$

Here E^{vac} is the total energy per unit cell of the surface-vacancy structure, $E^{\mathrm{Al\text{-}atom}}$ is the total energy of a free atom, and E_{coh} is the Al cohesive energy ($E_{\mathrm{coh}}=4.17$ eV for our slab). $E^{\mathrm{Al(111)}}$ is the total energy of the clean slab.

In the second process each vacancy is occupied by an alkali atom. Taking this process together with the vacancy formation energy gives the adsorption energy at the surface-substitutional site:

$$E_{\mathrm{ad}}^{\mathrm{Na/Al(111)\text{-}sub}}=E^{\mathrm{Na/Al(111)\text{-}sub}}-(E^{\mathrm{vac}}+E^{\mathrm{Na\text{-}atom}})+E_f^{\mathrm{vac}} . \tag{18}$$

Thus, when we discuss *adsorption energies* this takes into account that for the substitutional site the adsorption process has to pay a price to create a surface vacancy. On the other hand, the adsorbate *binding energy* is understood as the interaction of the adsorbed atom with the surface and it differs from E_{ad} by E_f^{vac} for the substitutional adsorption. For the "normal" adsorption the adsorption energy and the adatom binding energy are equal.

B. $(\sqrt{3}\times\sqrt{3})R30°$ Na on Al(111)

As the first example we investigate the $(\sqrt{3}\times\sqrt{3})R30°$ Na adlayer. In particular we will discuss the characteristic properties of different possible adsorption sites by studying the adsorption energy, work function, and the nature of the chemical bond. Figure 8 shows the calculated adsorption energies as a function of adsorbate height above the unrelaxed Al(111) surface for Na at the on-top, fcc, and substitutional positions. These energies were calculated according Eq. (16) for the "normal" on-surface sites and with Eq. (18) for the surface-substitutional site.

The formation energy of a $(\sqrt{3}\times\sqrt{3})R30°$ vacancy structure was calculated as $E_f^{\mathrm{vac}}=0.41$ eV [compare Eq. (17)] per surface vacancy. This vacancy formation energy may be compared with the formation energy of a distant surface Frenkel pair, where the removed Al atom is not at a step, but on a flat part of the Al(111) surface. For such a surface Frenkel pair we obtain a formation energy $E_f^{\mathrm{Frenkel}}=1.2$ eV. This *ab initio* result compares well with recent effective-medium theory results of Stoltze, Nørskov, and Landman,[35] who obtained 1.3 eV. For pro-

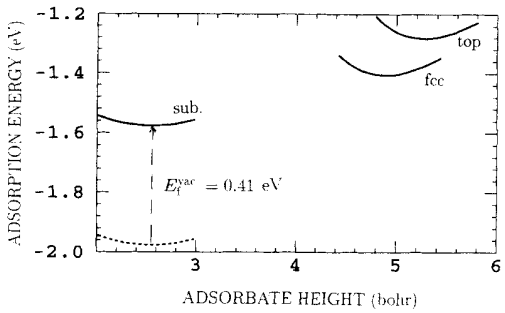

FIG. 8. Adsorption energies vs vertical distance between adsorbate and top-surface layer for a $(\sqrt{3}\times\sqrt{3})R30°$ Na overlayer adsorbed at the top, fcc, and substitutional sites. In this calculation the substrate atoms are not relaxed. The dashed line shows the binding energy for the substitutional adsorption relative to a surface-vacancy structure.

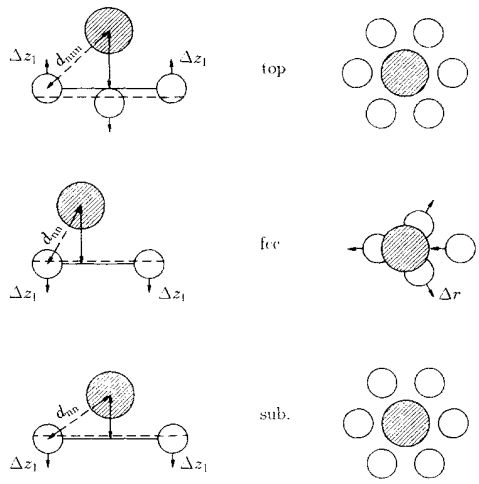

FIG. 9. Side view (left) and top view (right) of the atomic geometry after relaxation of the adsorbate and the top Al layer for the $(\sqrt{3}\times\sqrt{3})R30°$-Al(111) surface. The length scale of the left part is 1.4 of the right part. The hatched circles mark the Na atom and the open circles the Al-surface atoms. The calculated values of the atomic displacements are given in Table IV. The horizontal dashed line marks the position of the unrelaxed surface. The horizontal full line goes through the center of the relaxed outmost substrate atoms.

cesses related to surface melting and roughening this energy represents an important estimate for reaction barriers. For the adsorbate situation this energy is less important because the system already gains a higher energy by the adsorption process.

From the results of Fig. 8 we can estimate the $\bar{\Gamma}$-point phonon frequency (expressed in inverse centimeters) of an adatom vibration normal to the surface by

$$\nu=\frac{1}{2\pi c}\left[\frac{1}{m_{\rm ad}}\frac{\partial^2 E_{\rm ad}(z)}{\partial z^2}\right]^{1/2}. \tag{19}$$

$m_{\rm ad}$ is the atomic mass of the adsorbate and c is the velocity of light. For the $\bar{\Gamma}$-point phonon for the three sites this yields $\nu_{\rm top}=153$ cm^{-1}, $\nu_{\rm fcc}=150$ cm^{-1}, and $\nu_{\rm sub}=100$ cm^{-1}. The much softer mode for the substitutional adsorbate can be explained in terms of the larger bond angles of the adatom with the substrate atoms (see Fig. 9). The resulting energies of the zero-point vibrations ($\epsilon=\frac{1}{2}h\nu$) are $\epsilon_{\rm top}=9.3$ meV, $\epsilon_{\rm fcc}=9.5$ meV, and $\epsilon_{\rm sub}=6.4$ meV. With respect to experimental studies we note that these results should be taken with some caution because the adlayer was taken to vibrate against a rigid substrate. Preliminary studies which included the collective motion of the adatom and the two top substrate layers show that the phonon energies may be significantly reduced.

The calculations of the stable and metastable geometries show that the adsorbate-induced relaxation of the substrate atoms gives only a very small gain in binding energy. The qualitative behavior of the relaxation can be understood as that it tries to increase the effective coordination number of the adatom which can be realized by a decrease of the next-nearest-neighbor distance $d_{\rm nnn}$ (see Table IV and Fig. 9). The small energy gain of some tens of meV does not change the ordering of the total energies of the different adsorption sites in the case of Na on Al(111). The substrate relaxation energy gain is of the same order as the substrate phonon energies, which is in agreement with recent calculations of Feibelman for the Al adsorption on Al(100).[37] The strongest substrate relaxation is found for the on-top position, where the energy gain is 0.05 eV. The tendency to increase the adatom coordination number results in a hole digging which can be best seen for the on-top adsorption. Here the substrate atom below the adsorbate moves inward by 0.1 Å, and the six next-nearest neighbors move outward by 0.1 Å (see Fig. 9 and Table IV). By this substrate relaxation the distance between the Na adatom and its next-nearest-neighbor Al atoms is reduced by 4%. Since the nearest-neighbor bond length $d_{\rm nn}$ is nearly unchanged by the substrate relaxation it causes a reduction of the adsorbate height (vertical distance between adsorbate layer and the layer through the highest Al atoms) of about 0.2 Å, so that—after substrate relaxation—the height is practically identical for the fcc and on-top positions. This effect reduces the adsorbate-adsorbate repulsion because the substrate electrons can now penetrate to regions between Na atoms and thereby screen the direct Na-Na repulsion.

The calculated bond length between the Na adatom and its nearest-neighbor Al is 3.13 Å for the substitutional site. This compares reasonably well with the SEXAFS result of $d_{\rm nn}=3.31$ Å. The difference of 0.18 Å (or 5.4%) between the theoretical value and the SEXAFS result is larger than what we would have expected. This difference may be due several reasons: (1) The theoretical result is obtained for $T=0$ K. (2) Zero-point vibrations have been neglected. (3) The pseudopotential treatment is essentially equivalent to a frozen-core approximation. However, the repulsion between the core electrons with the substrate may be slightly inaccurate, because the Na $2p$ orbitals have quite a long range. (4) The differences may also indicate that the displaced Al atom has not moved away to a nearby step but is positioned between the Na adatoms. All these effects will increase the Na-substrate bond length. It is interesting to note that the

TABLE IV. Atomic geometry (compare Fig. 9) and energy gain due to substrate relaxation ΔE^{rel} for $(\sqrt{3}\times\sqrt{3})R30°$ Na on Al(111) with (rel) and without (unrel) relaxation of the two top Al layers. The directions of the atomic displacements are defined in Fig. 9.

site	surface	z_{ad} (Å)	Δz_1 (Å)	Δz_2 (Å)	Δr (Å)	d_{nn} (Å)	d_{nnn} (Å)	ΔE^{rel} (eV)
top	unrel	2.80				2.80	3.97	
top	rel	2.59	0.13	0.06		2.78	3.83	−0.05
fcc	unrel	2.61				3.07	4.17	
fcc	rel	2.61	0.01		0.02	3.08	4.15	−0.01
sub	unrel	1.31				3.11	3.96	
sub	rel	1.36	0.05			3.13	3.96	−0.01

effects (1)–(3) are also present in Na bulk calculations. Indeed, these calculations give a Na bcc lattice constant which is 4.5% smaller than the experimental lattice constant.[27]

Figure 10 shows the changes in bond length and binding energy as a function of the Na coordination number C_{Na}. The values of C_{Na} are 1, 3, and 6 for the on-top, fcc, and substitutional sites, respectively. The large increase of the bond length from the top position with coordination number 1 to the fcc site with coordination number 3 is consistent with the general experience that with increasing coordination number the bond length increases and the bond strength per bond decreases. Exceptions from this rule may occur, for example, for closed shell atoms (see, for example, Ref. 36), but such exceptions do not apply here. The calculated value of $\Delta d_{nn}=0.3$ Å agrees with the empirical result given by Kittel[38] as well as with the experimental value obtained by Over *et al.*[39] for Cs on Ru(0001) by their low-energy electron-diffraction (LEED) analysis for two different sites (three-fold hollow and on-top). The small change of the Na-Al bond length of 0.05 Å between the three-fold coordinated fcc position and the six-fold-coordination substitutional position does not, however, follow the same scaling. According to the empirical rule of Kittel a value of 0.2 Å would be expected [Fig. 10(a)]. This and the different gain in binding energy (Fig. 10) between the onefold- and threefold-coordinated and between the threefold- and sixfold-coordinated sites of 0.15 and 0.45 eV, respectively, indicate that the bonding mechanisms for the substitutional and "normal" adsorptions are quite different. This interpretation is also supported by the fact that all three adsorption sites (fcc hollow, on-top, and substitutional) give rise to a very similar work-function change, although the adsorbate-substrate distances are significantly different (see Table V). In Sec. III D we come back to this point and give a schematic description of the physics of the "normal" and the substitutional adsorption.

C. Comparison of $\Theta=\frac{1}{3}$ with $\Theta=\frac{1}{4}$

For low coverages one expects that the adsorbate-substrate (ad-sub) interaction dominates. This is certainly true for $\Theta\to 0$, which corresponds to isolated adatoms. When adsorbate-adsorbate (ad-ad) distances decrease the ad-ad interactions become stronger and for close-packed layers they may even dominate over the ad-sub interaction. In fact, Over *et al.*[39] found for the system Cs on Ru(0001) through LEED analysis that there is a change of the adsorption site from on-top to hollow as the coverage is increased from $\Theta=\frac{1}{4}$ to $\Theta=\frac{1}{3}$. Similar to our discussion they noted that the alkali-alkali interaction for different adsorption sites is screened differently, in particular if substrate atoms are located between neighboring adatoms.

In order to study the ad-ad interaction relative to the ad-sub interaction we will now compare a $\Theta=\frac{1}{4}$ overlayer in the 2×2 structure (see Fig. 7) and a $\Theta=\frac{1}{3}$ overlayer in the $(\sqrt{3}\times\sqrt{3})R30°$ structure. Because the ad-ad interaction is not necessarily a monotonic function of the ad-ad distance (the ad-ad interaction may even oscillate between being attractive and repulsive), the intended comparison is nontrivial. Several quantities, namely the adsorbate-substrate distance, the binding energy, and the

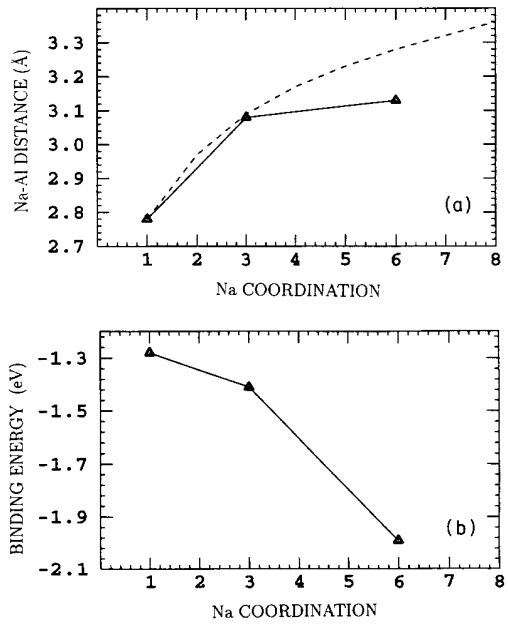

FIG. 10. Adsorbate-substrate bond length d_{nn} (a) and binding energy (b) vs the adatom coordination number. The dashed line connects empirical values given by Kittel (Ref. 38). The triangles are our calculated results.

TABLE V. Adsorption energy E_{ad}, adsorbate height z_{ad}, bond length d_{nn}, change in work function $\Delta\Phi$, dipole moment μ_D, and atomic radius of the adsorbate r_{ad} for Na and K in the $(\sqrt{3}\times\sqrt{3})$ and (2×2) structures on Al(111) for different adsorption sites. The formation energy of a surface vacancy is $E_f^{vac}=0.41$ eV and $E_f^{vac}=0.66$ eV for the $(\sqrt{3}\times\sqrt{3})R30°$ and (2×2) Al(111) structures, respectively. The atomic radius is calculated $r_{ad}=d_{nn}-r_{Al}$ with $r_{Al}=1.41$ Å (metallic radius of bulk Al). The adsorbate and the two top substrate layers are fully relaxed.

adsorbate	system	site	E_{ad} (eV)	z_{ad} (Å)	d_{nn} (Å)	$\Delta\Phi$ (eV)	μ_D (D)	r_{ad} (Å)
Na	$\sqrt{3}\times\sqrt{3}$	top	−1.28	2.59	2.78	−1.6	0.88	1.37
Na	$\sqrt{3}\times\sqrt{3}$	fcc	−1.41	2.61	3.08	−1.7	0.93	1.67
Na	$\sqrt{3}\times\sqrt{3}$	hcp	−1.42	2.58	3.06	−1.8	0.99	1.65
Na	$\sqrt{3}\times\sqrt{3}$	sub	−1.58	1.36	3.13	−1.6	0.88	1.72
Na	2×2	top	−1.32	2.54	2.73	−2.0	1.46	1.32
Na	2×2	fcc	−1.41	2.54	3.03	−2.1	1.53	1.62
Na	2×2	hcp	−1.42	2.54	3.02	−2.1	1.53	1.61
Na	2×2	sub	−1.46	1.31	3.11	−1.3	0.97	1.70
K	$\sqrt{3}\times\sqrt{3}$	top	−1.21	3.22	3.38	−1.6	0.88	1.97
K	$\sqrt{3}\times\sqrt{3}$	fcc	−1.20	3.28	3.67	−1.6	0.88	2.26
K	$\sqrt{3}\times\sqrt{3}$	sub	−1.17	2.39	3.70	−1.9	1.04	2.29
K	2×2	top	−1.18	3.16	3.32	−2.0	1.46	1.91
K	2×2	fcc	−1.19	3.22	3.61	−2.0	1.46	2.20
K	2×2	sub	−0.97	2.34	3.66	−2.2	1.64	2.25

local adsorbate dipole moment, provide important information about the nature of these interactions. Because all three quantities when analyzed as a function of the ad-ad distance give the same physical picture, we tend to accept inferences that can be drawn by making this comparison.

The results of Table V show that the work-function change for fcc-hollow-site adatoms changes from $\Delta\Phi=-2.1$ to -1.7 eV when the coverage is increased from $\Theta=\frac{1}{4}$ to $\Theta=\frac{1}{3}$. This means that the dipole moment per adatom changes from 1.53 to 0.93 D. Thus the depolarization is significant, namely reducing the $\Theta=\frac{1}{4}$ dipole moment by 40%. On the other hand, for the substitutional adsorbate we find that the dipole moment changes from 0.97 to 0.88 D. Thus the depolarization is only 9%, much smaller than for "normal" adsorption. This result indicates that the ad-ad interaction is well screened for the substitutional adsorbate.

The change of the Na-Al distance with decreasing Na-Na distance is +0.05 Å for the "normal" adsorption and 0.02 Å for the substitutional adsorption. This again supports the idea of a partially ionic bonding: As the ionic degree decreases with coverage, the bond length gets longer. Because the depolarization is larger for the on-surface adsorption, the change of the bond length is larger in this case as well. Our calculated increase of bond length with increasing coverage may be compared with experimental results by Lamble *et al.*,[40] who found for Cs on Ag(111) an increase of bond length of 0.3 Å for a coverage increase from $\Theta=0.15$ to 0.3. A quantitative comparison of this value with ours is not possible because the coverages as well as the systems are different.

With our theoretical results we can understand why the bond length $d_{nn}(C_{Na})$ does not follow the dotted curve of Fig. 10. In going from coordination number $C_{Na}=3$ to $C_{Na}=6$ the bond length is expected to increase by about 0.2 Å—if the ionic degree of the substitutional adsorbate remains constant. However, the substitutional Na adsorbate is much less depolarized than the on-surface adsorption. Thus the substitutional Na is more ionic, which tends to reduce the bond length. The higher degree of ionicity also follows from the large dipole moment, which is comparable to that of the fcc adsorbate, although the adsorbate-substrate distance is halved.

Comparing the binding energies for different adsorbate coverages we find that the ad-ad interaction depends strongly on the adsorbate site—for the on-top position we get a net repulsion; for the fcc site, repulsive and attractive interactions apparently cancel each other; and for the substitutional site there is a net attractive interaction. Therefore the formation of $(\sqrt{3}\times\sqrt{3})R30°$ adsorbate islands is the energetically most favorable structure for average coverages $\Theta\leq\frac{1}{3}$ and substitutional adatoms.

The result that the ad-ad interaction for surface-substitutional adatoms is attractive although the *direct* dipole-dipole interaction is repulsive is, at first glance, surprising. It is due to the difference in the formation energy of surface vacancies in the $(\sqrt{3}\times\sqrt{3})R30°$ and the 2×2 structure. The calculated vacancy formation energies are $E_f^{vac}=0.41$ eV and $E_f^{vac}=0.66$ eV, respectively. This increase of the formation energy with increasing distance of the surface vacancies does not follow the trend predicted by a bond-cutting model: A bond-cutting model with $E(C_{Al})=E_0-A\sqrt{C_{Al}}+BC_{Al}$ as proposed by Robertson, Payne, and Heine,[41] and using the values obtained by Methfessel, Hennig, and Scheffler,[36] gives $E_f^{vac}=0.96$ eV for $(\sqrt{3}\times\sqrt{3})R30°$, 0.89 eV for a (2×2) structure, and 0.82 eV for the isolated vacancy. In the bond-cutting model the energy per surface vacancy has to increase with decreasing vacancy-vacancy distance. This prediction is contradicted by the full calculations, which show that the $(\sqrt{3}\times\sqrt{3})R30°$ structure has a rather low

energy. We understand this result as very special property of this structure and of the valence electrons of aluminum. The arrangement of the surface Al atoms in the $(\sqrt{3}\times\sqrt{3})R30°$ structure is that of a graphite layer. In such an arrangement group-III atoms with three valence electrons are preferred.

D. Analysis of the bonding mechanism

In the previous Sec. III C we pointed out that the preference and the properties of the substitutional adsorption can be understood in terms of substrate-mediated screening of the direct Na-Na electrostatic repulsion. To analyze the screening behavior in more detail we investigated the adsorbate-induced electron density. A detailed analysis of the electronic states (orbital character and surface band structure) will be published elsewhere.[42] This analysis fully supports the nature of bonding described here.

A comparison of the electron density at the surface shows that the surface corrugation for the substitutional adsorption is much stronger than for the "normal" adsorption [see Figs. 11(a)–11(c)]. However, this strong density corrugation is not a result of the adsorbate electronic states, but essentially due to the surface vacancies. Figure 11 reveals clearly that the substrate electron density between two adsorbate atoms is much larger for the substitutional than for the "normal" adsorption. This large electron density obviously will screen the ad-ad interaction.

In order to visualize the adsorbate-induced perturbation of the surface electron density we show in Figs. 11(d)–11(f) the difference in charge density between the adsorbate system and a reference system. The reference system for the on-top and the fcc adsorption is the clean surface, and for the substitutional adsorption we use the vacancy structure. For the "normal" adsorption we find that the charge density changes take place in front of the top Al-substrate layer—the maximum is between the adsorbate and the top substrate layer [Figs. 11(d) and 11(e)]. Inside the substrate the charge-density change is very small. The substitutional adsorption shows a different behavior. Due to the vacancy structure, which represents a very open surface, the charge perturbation reaches somewhat deeper into the substrate [Fig. 11(f)]. This behavior is better seen in the xy-averaged charge-density change $\Delta\hat{n}(z)=\hat{n}(z)^{\mathrm{Na/Al(111)}}-\hat{n}^{\mathrm{ref}}(z)$ which is shown in Fig. 12. In order to see the long-range character of the Friedel-like oscillations we showed this change for ten-layer slabs. For the "normal" adsorption there is a minimum of $\Delta\hat{n}(z)$ at the top Al layer, indicating that the close-packed surface is the border for charge transfer, whereas for the substitutional the minimum is nearly at the second substrate layer.

Inside the metallic slab the only charge-density changes are Friedel-like oscillations, which very rapidly screen the changes in potential due to the adsorbate. The wavelength of these Friedel oscillations of 3.3 bohr agrees well with 3.34 bohr which follows for a free-electron gas with density $r_s=2.04$ bohr. This r_s value corresponds to aluminum, i.e., to a fcc metal with $a_0=7.53$ bohr and

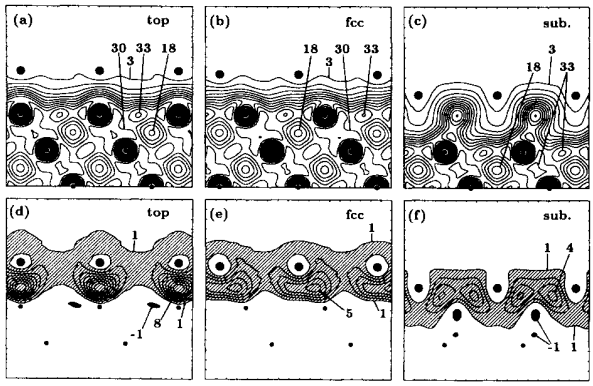

FIG. 11. Electron density (a), (b), (c), and induced electron density (d), (e), (f) for the $(\sqrt{3}\times\sqrt{3})R30°$-Na adlayer at different adsorption sites. The plane of the contour plots is normal to the surface and parallel to the $[1\bar{2}1]$ axis. The electron charge-density change for the top and fcc site is the difference between the density of the Na-adsorbed system and the clean surface [(d) and (e)], and for the substitutional site we show the difference between the adsorbate system and the corresponding vacancy structure. The substrate Al atoms are indicated by small dots and the Na adsorbate by large dots. Units are in 10^{-3} bohr^{-3}.

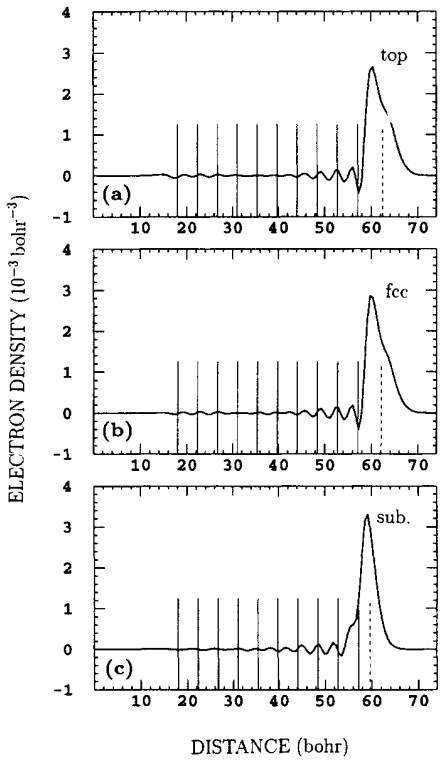

FIG. 12. xy-averaged charge-density change $[\Delta\hat{n}(z)=\hat{n}^{\mathrm{Na/Al(111)}}-\hat{n}^{\mathrm{ref}}(z)]$ for Na at the (a) on-top, (b) fcc, and (c) substitutional sites. The full vertical lines mark the positions of the Al layers in the slab, the vertical dashed line the position of the Na overlayer. The induced dipole moment which determines the change in the work function is nearly the same for all these adsorption sites. Note the Friedel oscillations which rapidly decay into the slab.

three valence electrons per atom. The main maximum of the adsorbate-induced charge density is nearly independent on the position of the adsorbate. This indicates that the induced charge density is essentially a substrate effect, i.e., due to an imagelike screening of the adatoms, and it is little affected by hybridization of the adsorbate with substrate orbitals.

IV. K ON Al(111)

To learn about chemical trends of alkali adsorbates we investigated the adsorption of K on Al(111). The main differences between the two alkali metals Na and K are the metallic radius ($r^{K}=2.26$ Å, $r^{Na}=1.83$ Å) and the ionization energies ($I^{Na}=5.14$ eV, $I^{K}=4.34$ eV).[34] As a consequence of the larger atomic radius K will have a bigger distance from the surface, which implies that it experiences a rather small substrate electron-density corrugation. Therefore we find for the unrelaxed surface that for K the on-top and fcc positions are closer in energy than for Na (see Fig. 13 and compare it with Fig. 8). If the substrate relaxation is included the energy of the on-top position becomes degenerate (within our numerical accuracy) with the energy of the fcc site (see Table V). The comparison of our results for Na and for K are very interesting: Whereas the on-top position was clearly unfavorable for Na it is now possible for K. This trend is expected also to hold for larger alkalis. The preference of the on-top position with similar distortions as we calculated were experimentally obtained by a LEED analysis from Fisher *et al.*[43] for the system K/Ni(111).

Also, the adsorption energy for the substitutional site of $(\sqrt{3}\times\sqrt{3})R30°$ K is very close to that of the other sites. From our total-energy calculation we therefore do not dare to draw definite conclusions about the K adsorption site. The preference of the substitutional site thus is less pronounced for bigger alkalis, because the formation energy of a surface vacancy remains constant but the adsorbate-substrate interaction gets weaker because of the bigger distance. Furthermore, larger alkali adatoms cannot be as deeply bound in vacancies as Na. This makes the substrate-mediated screening of the ad-ad interaction less efficient and therefore increases the repulsive and/or depolarizing dipole-dipole interaction.

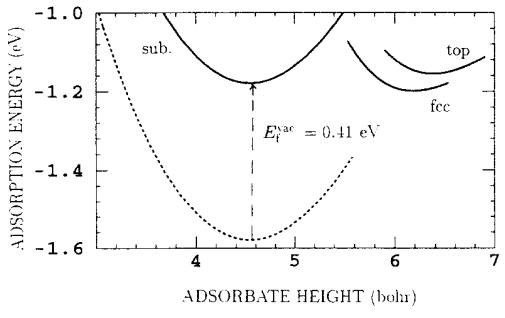

FIG. 13. Adsorption energies vs the vertical distance between the adsorbate and the top-surface layer for a $(\sqrt{3}\times\sqrt{3})R30°$ K overlayer adsorbed at the top, fcc, and substitutional sites. In this calculation the substrate atoms are not relaxed. The dashed line shows the binding energy for the substitutional adsorption relative to the corresponding vacancy structure.

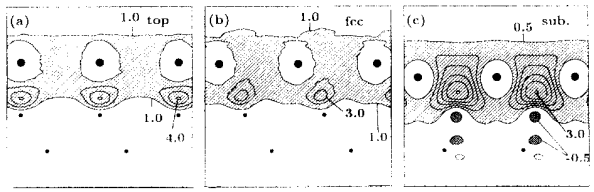

FIG. 14. Electron-density change $(\sqrt{3}\times\sqrt{3})R30°$ K on Al(111) adsorbed at the (a) on-top, (b) fcc, and (c) substitutional sites. For the on-top and fcc sites the reference system is the clean Al surface. For the substitutional site the reference system is the surface-vacancy structure. The figure shows contours in the plane normal to the surface and parallel to the $[1\bar{2}1]$ axis (see also Fig. 7). The substrate Al atoms are indicated by small dots, the K adsorbate by large dots. Units are 10^{-4} bohr^{-3}.

As in Sec. III C for Na adsorption, we investigated the changes in binding energy, adsorbate-substrate bond length, and work-function change by decreasing the coverage from $\Theta=\frac{1}{3}$ to $\Theta=\frac{1}{4}$ (see Table V). Comparing the adsorption energies we find that the ad-ad interaction is attractive for all three sites, but for the on-top and fcc positions the energy differences are within our numerical accuracy. The change of the K-Al distance with coverage is 0.06 Å for the "normal" adsorption and 0.04 Å for the

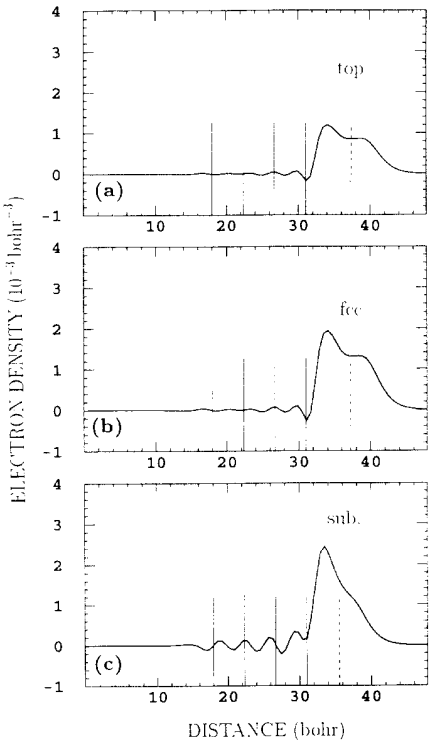

FIG. 15. *xy*-averaged adsorbate-induced charge density as a function of distance perpendicular to surface for K on the (a) top, (b) fcc, and (c) substitutional sites. The solid vertical lines mark the positions of the Al layers in the slab, the vertical dashed line the position of the K overlayer.

substitutional adsorption, i.e., a similar behavior as that found for the Na-Al distance. The results of Table V show that the work-function change as well as the dipole moment for "normal" and substitutional adsorption increases. The drastic increase of the dipole moment for the substitutional site with local coverage, which is in contradiction to what we found for the Na adsorption, can be explained by a weaker screening of the repulsive ad-ad interaction, since the K adsorbate is higher above the substrate surface and therefore the substrate-mediated screening density between the adatoms is smaller.

In the same way as described in Sec. III B we calculated the phonon frequencies for $(\sqrt{3}\times\sqrt{3})$ K on Al(111) (Fig. 13). The frequencies are $\nu_{\text{top}}=108$ cm^{-1}, $\nu_{\text{fcc}}=91$ cm^{-1}, and $\nu_{\text{sub}}=128$ cm^{-1} for the on-top, fcc, and substitutional sites, respectively, i.e., they are much softer than for Na on the $(\sqrt{3}\times\sqrt{3})$ Al(111) surface. This can be understood in terms of the charge redistribution. Compared to the corresponding redistribution of Na on the Al surface, the maximum density is lower and the redistribution occurs over a large region (Figs. 14 and 15). This is a direct result of the larger atomic radius of K. The maximum of the averaged charge redistribution (Fig. 15) is nearly at the same location as it is for Na on Al(111). This again shows that this position is determined by the metallic substrate and not by the adsorbate.

V. CONCLUSIONS

In this paper we discussed detailed density-functional theory slab calculations for various configurations of Na and K adlayers on Al(111). We studied different adsorbate meshes as well as different adsorbate sites.

We gave a detailed discussion of our method which enables us to take general electrostatic fields into account. Through this method, a direct investigation of adsorbates under the influence of electric fields such as those occurring in field-ion and scanning-tunneling microscopy becomes feasible. In this paper we used this approach to implement a dipole correction which enables a reduction of the slab thickness by placing the adsorbate only on one side of the slab. Although many calculations are performed using a four-layer slab, we ensured the accuracy of our results by performing several tests and by repeating the most important studies with a ten-layer substrate.

In this paper we presented theoretical evidence that alkali atoms on the close-packed Al(111) surface can adsorb at "unusual" adsorption sites, namely on-top and substitutional. The latter position implies that each adatom kicks out a substrate surface atom and takes—in a more or less ideal way—its position. Because of the mismatch of atomic radii the substitution is obviously not perfect. We explain the hitherto-unexpected result of the preference of the substitutional site by the low formation energy of the surface vacancies and by a substrate-mediated screening of the direct adsorbate-adsorbate electrostatic repulsion. We find that the adatom at the substitutional site behaves similarly to an isolated adatom and the ionic type of bonding can develop most strongly. This is different for the "normal," i.e., on-surface adsorbate geometries, where at $\Theta=\frac{1}{4}$ the depolarization is already significant. Despite the strong ionic character of the substitutional adsorbate we find that the adsorbate-adsorbate interaction is net attractive and that the formation of a $(\sqrt{3}\times\sqrt{3})R30°$ structure is energetically preferred over more distant adsorbate arrangements, e.g., the $(2\times2)\Theta=\frac{1}{4}$ adlayer. Thus, for an average coverage $\Theta\leq\frac{1}{3}$ we predict island formation with a $(\sqrt{3}\times\sqrt{3})R30°$ unit cell. This result is explained as a property of the formation of surface vacancies rather than as a result of the adsorbate-adsorbate interactions. In contrast to Na, where the on-top position is energetically clearly unfavorable, we find that it becomes possible for potassium. This result is explained as a consequence of the energy gain due to substrate relaxation for the on-top position and the bigger size of K, which implies that the adatom experiences a rather small substrate electron-density corrugation.

Some open questions remain. For example, we are unable at this time to predict the details of the reaction path through which the surface aluminum atom is kicked out in the process of the substitutional adsorption.

ACKNOWLEDGMENTS

The authors are grateful to H. Brune, R. Diehl, and R. Stumpf for stimulating discussions.

[1] J. W. Döbereiner, *Zur Chemie des Platins in wissenschaftlicher und technischer Beziehung* (Balz'sche Buchhandlung, Stuttgart, 1836).
[2] J. W. v. Goethe, in *Döbereiner, Goethe und die Katalyse,* edited by A. Mittasch (Hippokrates, Stuttgart, 1952), p. 29.
[3] J. B. Taylor and I. Langmuir, Phys. Rev. **44**, 423 (1933).
[4] R. W. Gurney, Phys. Rev. **47**, 479 (1935).
[5] *Physics and Chemistry of Alkali Metal Adsorption,* edited by H. P. Bonzel, A. M. Bradshaw, and G. Ertl (Elsevier, Amsterdam, 1989).
[6] J. P. Muscat and D. M. Newns, Surf. Sci. **84**, 262 (1979).
[7] N. D. Lang and A. R. Williams, Phys. Rev. B **18**, 616 (1978).
[8] M. Scheffler, Ch. Droste, A. Fleszar, F. Máca, G. Wachutka, and G. Barzel, Physica B **172**, 143 (1991).
[9] N. D. Lang, Phys. Rev. B **4**, 4234 (1971).
[10] H. Ishida and K. Terakura, Phys. Rev. B **38**, 5752 (1988).
[11] H. Ishida, Phys. Rev. B **42**, 10 899 (1990).
[12] D. M. Riffe, G. K. Wertheim, and P. H. Citrin, Phys. Rev. Lett. **64**, 571 (1990).
[13] S. Modesti, C. T. Chen, Y. Ma, and G. Meigs, P. Rudolf, and F. Sette, Phys. Rev. B **42**, 5381 (1990).
[14] G. A. Benesh and D. A. King, Chem. Phys. Lett. **191**, 315 (1992).
[15] A. Schmalz, S. Aminpirooz, L. Becker, J. Haase, J. Neugebauer, M. Scheffler, D. R. Batchelor, D. L. Adams, and E. Bøgh, Phys. Rev. Lett. **67**, 2163 (1991).
[16] J. N. Andersen, M. Qvarford, R. Nyholm, J. F. van Acker, and E. Lundgren, Phys. Rev. B **68**, 94 (1992).
[17] D. M. Ceperley and B. J. Alder, Phys. Rev. Lett. **45**, 566 (1980).

[18]J. Perdew and A. Zunger, Phys. Rev. B **23**, 5048 (1981).
[19]X. Gonze, R. Stumpf, and M. Scheffler, Phys. Rev. B **44**, 8503 (1991); R. Stumpf, X. Gonze, and M. Scheffler (unpublished).
[20]L. Kleinman and D. M. Bylander, Phys. Rev. Lett. **48**, 1425 (1982).
[21]H. J. Monkhorst and J. D. Pack, Phys. Rev. B **13**, 5188 (1976).
[22]V. L. Moruzzi, J. F. Janak, and A. R. Williams, *Calculated Electronic Properties of Metals* (Pergamon, New York, 1978).
[23]B. Chakraborty and R. W. Siegel, Phys. Rev. B **27**, 4535 (1983).
[24]D. J. Chadi and M. L. Cohen, Phys. Rev. B **8**, 5747 (1973).
[25]S. G. Louie, S. Froyen, and M. L. Cohen, Phys. Rev. B **26**, 1738 (1982).
[26]J. Hebenstreit, M. Heinemann, and M. Scheffler, Phys. Rev. Lett. **67**, 1031 (1991).
[27]J. Hebenstreit and M. Scheffler, Phys. Rev. B **46**, 10 134 (1992).
[28]See, e.g., L. E. Reichl, *A Modern Course in Statistical Physics* (Edward Arnold, Austin, TX, 1987).
[29]M. J. Gillan, J. Phys. Condens. Matter **1**, 689 (1989).
[30]R. Car and M. Parrinello, Phys. Rev. Lett. **55**, 2471 (1985).
[31]R. Stumpf and M. Scheffler (unpublished).
[32]C. J. Todd and T. N. Rhodin, Surf. Sci. **42**, 109 (1974).
[33]J. E. Inglesfield, Surf. Sci. **188**, 1701 (1987); G. C. Aers and J. E. Inglesfield, *ibid.* **217**, 367 (1989).
[34]N. W. Ashcroft and N. D. Mermin, *Solid State Physics* (HRW International Editions, Philadelphia, 1976).
[35]P. Stoltze, J. K. Nørskov, and U. Landman, Phys. Rev. Lett. **61**, 440 (1988).
[36]M. Methfessel, D. Hennig, and M. Scheffler, Appl. Phys. A **55**, 442 (1992).
[37]P. Feibelman, Phys. Rev. Lett. **65**, 729 (1990).
[38]C. Kittel, *Introduction to Solid State Physics* (Wiley, New York, 1986).
[39]H. Over, H. Bludau, M. Skottke-Klein, G. Ertl, W. Moritz, and C. T. Campbell, Phys. Rev. B **45**, 8658 (1992).
[40]G. M. Lamble, R. S. Brooks, D. A. King, and D. Norman, Phys. Rev. Lett. **61**, 1112 (1988).
[41]I. J. Robertson, M. C. Payne, and V. Heine, Europhys. Lett. **15**, 301 (1991).
[42]B. Wenzien, J. Neugebauer, J. Bormet, and M. Scheffler (unpublished).
[43]D. Fisher, S. Chandavarkar, I. R. Collins, R. D. Diehl, P. Kaukasoina, and M. Lindroos, Phys. Rev. Lett. **68**, 2786 (1992).

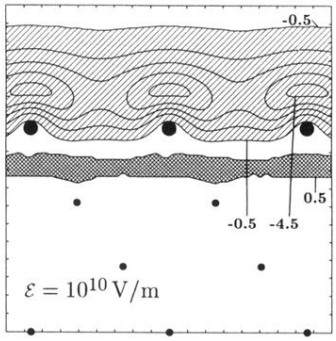

FIG. 5. Electron-density change $\Delta\hat{n}(z)$ induced by an electrostatic field $\mathcal{E}=10^{10}$ V/m for $(\sqrt{3}\times\sqrt{3})R\,30°$ Na on Al(111) (substitutional site). The figure shows contours in the plane lying normal to the surface and parallel to the $[1\bar{2}1]$ axis (see also Fig. 7). Contours are separated by 0.5×10^{-4} bohr^{-3}. The substrate Al atoms are indicated by small dots, the Na adsorbate by large dots. The contour units are 10^{-4} bohr^{-3}.

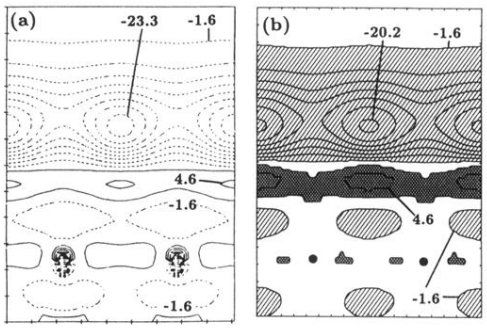

FIG. 6. Comparison of the screening charge densities calculated by (a) Inglesfield (Ref. 33) and (b) by us for the Al(100) surface. The external electric field is $\mathcal{E}=5.14\times10^{9}$ V/m. The figure shows contours in the plane lying normal to the surface which intersects the atoms in the second surface layer. The first contours are $\pm1.6\times10^{-5}$ bohr^{-3}. Contours are separated by 3.1×10^{-5} bohr^{-3}. In (a) dashed contours indicate negative electron density and the solid contours positive density. For our calculation we used a ten-layer Al substrate. The atomic positions are marked by dots.

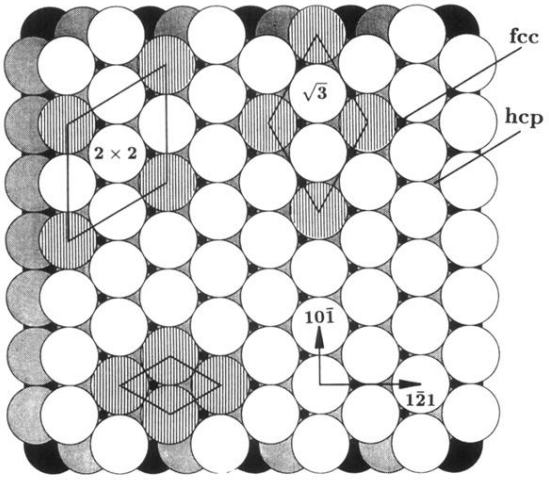

FIG. 7. The (1×1), $(\sqrt{3}\times\sqrt{3})R30°$, and (2×2) surface unit cells of Al(111). White, grey, and black circles show the top, second, and third layer of Al. Edge atoms of the three unit cells are hatched. Furthermore, the fcc and hcp on-surface adsorption sites are indicated.